

# Chapter 4

## Dynamic Model of the CHS

### 4.1 Mechanics of Track-Terrain Interaction

There are many approaches used to study and explain a phenomenon that occurs beneath tracks while a tracked vehicle is running over terrain; nevertheless, some approaches such as those employing the theory of plastic equilibrium or the finite element method involve an extensive and burdensome amount of numerical computation. This leads to the requirement for a high-speed computer, and, of course, brings about a potential cost problem. Moreover, to be able to apply existing control theories for designing a system controller, the model of the CHS has to be kept as simple as possible, yet still adequately represent the principal behaviors of the system. As a result, a fairly simple model of the track-terrain interaction using the semiempirical method is chosen, and will be discussed in detail as follows.

#### 4.1.1 Terrain Model

By observing and studying shear stress-displacement characteristics, terrain can be categorized into two major types. One, called “Brittle Soil”, displays a maximum shear stress  $\tau_{max}$  and a flattened portion of residual shear stress  $\tau_r$  after yielding of the soil at point  $j_0$ , as shown by curve 1 in Fig. 4.1. Undisturbed firm soils, such as dense sand, silt and loam, and frozen snow may exhibit these characteristics. The other, called “Plastic Soil”, exhibits a smooth shear stress-displacement characteristic, and the shear stress does not fall off after the maximum, as shown by curve 2 in Fig. 4.1. Loose soils, such as loose sand, saturated clay, dry snow, and most disturbed soils are of this type [Wong, 1978].

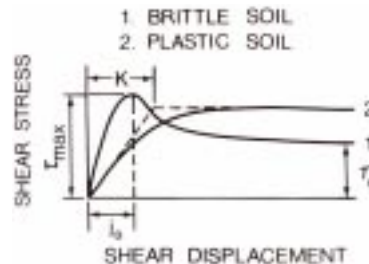


Figure 4.1. Two types of shear stress-shear displacement characteristic

In a coal mine, the floor condition varies widely from mud to hard ground. However, the ground condition often found in the coal mine is hard surface covered by a fairly thick layer of coal dust. The coal dust comprises gravel-like fine-grained sand; therefore, it will be classified as a kind of plastic soil. For this kind of terrain, the following shear stress-displacement relationship, based on Mohr-Coulomb failure criterion, can be used [Bekker, 1969].

$$\begin{aligned}\tau &= (c + \sigma \tan \phi)(1 - e^{-j/K}) \\ &= \tau_{\max} (1 - e^{-j/K})\end{aligned}\tag{4.1}$$

where  $c$  = apparent cohesion of the soil

$\sigma$  = normal stress on the sheared surface

$\phi$  = angle of internal shearing resistance of the soil

$K$  = shear deformation modulus

$j$  = shear displacement

The derivation of the above relationship is based on the assumptions that the soil is homogeneous and behaves as a rigid-perfectly plastic material. That is, the soil is rigid under increasing loads until a stress condition at which failure occurs is reached, and then undergoes plastic flow. No recoverable elastic deformation occurs [Le, et al., 1997]. These soil parameters,  $c$ ,  $\phi$ , and  $K$ , for any soil types can be determined from field tests.

#### 4.1.2 Normal Pressure Distributions under Tracks

To be able to compute the amount of traction produced by a track, we need to know how the normal pressure beneath the track is distributed. In Fig. 4.2, all forces acting on an MBC under normal operating condition are shown. These forces comprise the weights of the MBC and the Dolly, the interacting forces occurring at the Dolly's connecting pin and the rear doughnut, and the ground forces exerted on the tracks. All other inertia forces, occurring at the centers of mass of the MBC and the Dolly due to accelerations, are neglected since each MBC in the CHS is operated at low speed and acceleration. Thus, the normal pressure distributions,  $p_R(x)$  and  $p_L(x)$  (not shown in the figure), can be simply determined by enforcing a static equilibrium condition.

According to the design of the running gear of the MBC, a shearing plate is used to bear and distribute the MBC load on each track. The normal pressure distributions under the MBC's tracks can be assumed to be linear as shown in Fig. 4.3.

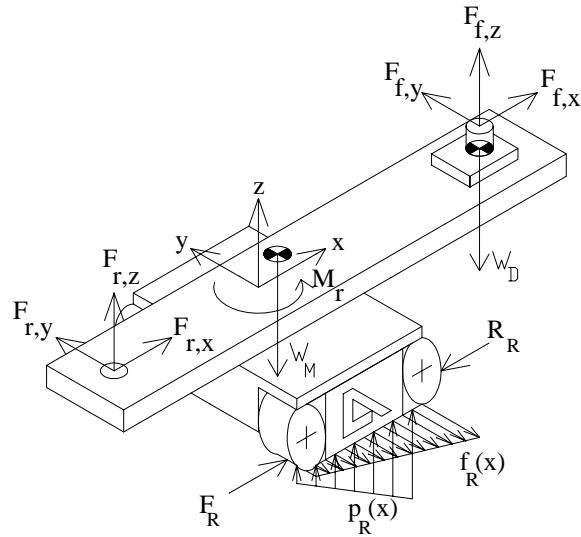


Figure 4.2. Forces Acting on an MBC during Operation

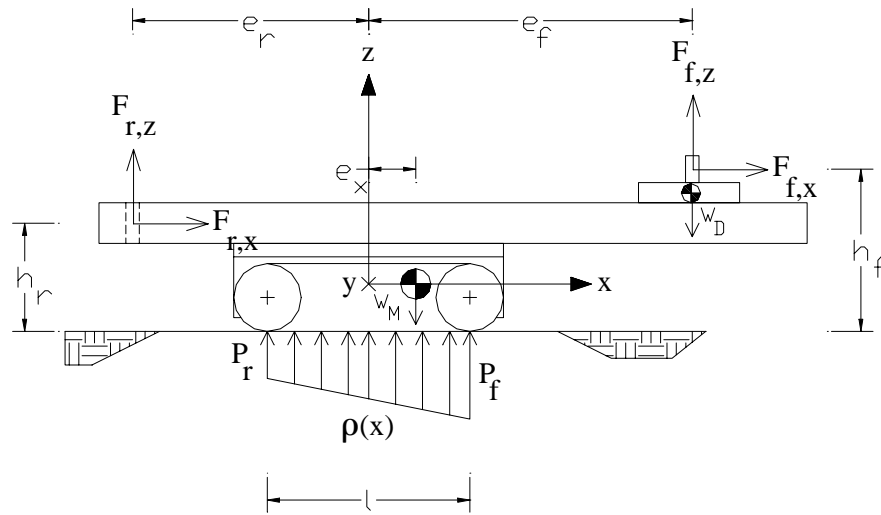


Figure 4.3. Side View of an MBC

A side view of the MBC and all geometric parameters needed for calculating the normal pressure distribution are shown in Fig. 4.3. Due to the much greater weight of the

MBC,  $W_M$ , compared to that of the Dolly,  $W_D$ , one may lump the weight of the Dolly to the weight of the MBC and consider it as single weight acting through the center of gravity of the MBC.

From Fig. 4.3, the line load,  $p(x)$ , can be written in the general form as follows:

$$p(x) = \frac{P_f - P_r}{l}x + \frac{P_f + P_r}{2} \quad (4.2)$$

To determine the values of  $P_f$  and  $P_r$ , we start by assuming that the MBC's weight shifts forward or backward only along the x-axis, and no weight shifting occurs along the y-axis. In this case,  $p_R(x)$  and  $p_L(x)$  have the same expression, and are equal to  $p(x)/2w$ .

Summing forces along the z-axis and moments around the center point of the contact area between tracks and ground, we have

$$\sum F_z = 0; \quad \int_{-l/2}^{l/2} p(x)dx + F_{f,z} + F_{r,z} - W_M = 0 \quad (4.3)$$

$$\sum M_y = 0; \quad -\int_{-l/2}^0 xp(x)dx - \int_0^{l/2} xp(x)dx - F_{f,z}e_f + F_{f,x}h_f + F_{r,z}e_r + F_{r,x}h_r + W_Me_x = 0 \quad (4.4)$$

Substituting Eq. 4.2 into Eqs. 4.3 and 4.4, and solving for  $P_f$  and  $P_r$ , we obtain

$$P_f = \frac{(W_M - F_{f,z} - F_{r,z})}{l} + \frac{6}{l^2}(F_{f,x}h_f + F_{r,z}e_r + F_{r,x}h_r + W_Me_x - F_{f,z}e_f) \quad (4.5)$$

$$P_r = \frac{(W_M - F_{f,z} - F_{r,z})}{l} - \frac{6}{l^2}(F_{f,x}h_f + F_{r,z}e_r + F_{r,x}h_r + W_Me_x - F_{f,z}e_f) \quad (4.6)$$

Next, we account for the effect of the MBC's weight shift along the y-axis of the normal pressure distribution. From Fig. 4.4, the values of  $P_R$  and  $P_L$  must be determined,

and included in  $p(x)/2w$  to obtain the expressions of  $p_R(x)$  and  $p_L(x)$ , respectively. By summing moments in the x-axis around the origin of the coordinate system, we have

$$\sum M_x = 0; \quad P_L - P_R = \frac{2(F_{f,y}h_f + F_{r,y}h_r + W_M e_y)}{B} \quad (4.7)$$

Since  $P_R$  and  $P_L$  are present to counteract the moment due to the weight shift and the forces in the y-axis, they form a couple. Thus, substituting  $P_R = -P_L$  in Eq. 4.7, the expressions for  $P_R$  and  $P_L$  can be determined from:

$$P_R = -\frac{(F_{f,y}h_f + F_{r,y}h_r + W_M e_y)}{B} \quad (4.8)$$

$$P_L = \frac{(F_{f,y}h_f + F_{r,y}h_r + W_M e_y)}{B} \quad (4.9)$$

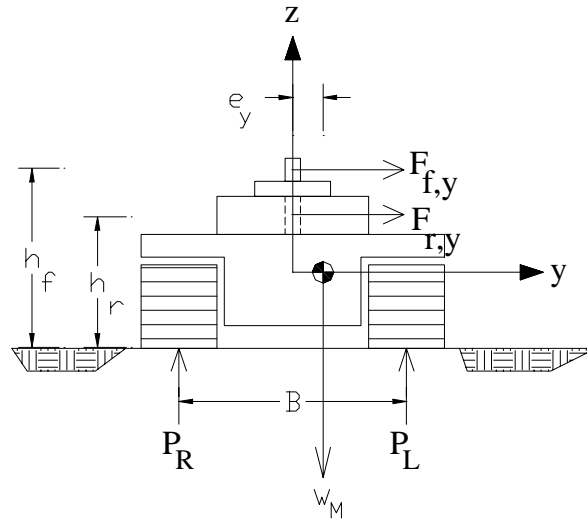


Figure 4.4. The Front View of an MBC

Finally, the complete expressions for the normal pressure distribution under each track,  $p_R(x)$  and  $p_L(x)$ , are:

$$p_R(x) = \frac{p(x)}{2w} + \frac{P_R}{lw} \quad (4.10)$$

$$p_L(x) = \frac{p(x)}{2w} + \frac{P_L}{lw} \quad (4.11)$$

#### 4.1.3 Tractive Effort and Slip of a Track

The tractive effort of a track is produced by the shearing of the terrain surface. It varies with the terrain type and the amount of track slip. The total tractive effort of a track can be calculated as follows:

$$F = \text{sign}(V_t - V) \bullet w \int_{-l/2}^{l/2} \tau dx \quad (4.12)$$

where  $V$  = the velocity of the track relative to the ground

$$= v_x \pm \frac{\omega B}{2}, \quad (+) \text{ for the right track}$$

(-) for the left track

$V_t$  = the velocity of the track relative to the MBC's hull

Substituting Eq. 4.1 into Eq. 4.12, we obtain

$$F = \text{sign}(V_t - V) \bullet w \int_{-l/2}^{l/2} (c + \sigma \tan \phi)(1 - e^{-j/K}) dx \quad (4.13)$$

The slip of a track,  $i$ , is defined as follows:

$$i = 1 - \frac{V}{V_t}, \quad \text{when } V_t \neq 0 \quad (4.14)$$

The relationship between the shear displacement,  $j$ , and the slip of a track,  $i$ , is:

$$j = |i| \left( \frac{l}{2} - \text{sign}(V_t) \bullet x \right) \quad (4.15)$$

Thus, Eq. 4.13 can be rewritten in the following form:

$$F = \text{sign}(V_t - V) \bullet w \int_{-l/2}^{l/2} (c + \sigma \tan \phi) (1 - e^{-\left(|i|\left(\frac{l}{2} - \text{sign}(V_t) \bullet x\right)/K\right)}) dx \quad (4.16)$$

where  $\sigma = p_R(x)$  for the right track

and  $\sigma = p_L(x)$  for the left track

In the case of  $V_t = 0$  but  $V \neq 0$ , the tractive effort is maximum, and can be calculated from:

$$F_{\max} = \text{sign}(V_t - V) \bullet w \int_{-l/2}^{l/2} (c + \sigma \tan \phi) dx \quad (4.17)$$

#### 4.1.4 Terrain Resistance

While a tracked vehicle is maneuvering over terrain, the tractive effort generated by both tracks must overcome the terrain resistance to allow the vehicle to move. As shown in Fig. 4.2, there are three kinds of terrain resistance; longitudinal resistance( $R$ ), lateral resistance( $f(x)$ ), and the moment of turning resistance( $M_r$ ). Each of them is discussed in detail as follows.

##### *Longitudinal Resistance, R:*

The MBC is usually operated on hard ground. Therefore, the effect of bulldozing resistance, which occurs when a tracked vehicle is operated on soft ground and the running gear sinks into the ground, can be neglected. In this study, the longitudinal resistance will be model as friction force occurring between the track and the ground, and given by

$$R = \text{sign}(V) \bullet \mu_x w \int_{-l/2}^{l/2} \sigma dx \quad (4.18)$$

where  $\mu_x$  = the longitudinal friction coefficient

The direction of the longitudinal resistance is opposite to the direction of the actual velocity ( $V$ ) of the track.

*Lateral Resistance,  $f(x)$ :*

When a tracked vehicle turns or has a sideslip motion, there will be lateral slippage of the track, which leads to a lateral resistance. According to Wong [1978], the lateral resistance per unit length of the track,  $f(x)$ , can be expressed by

$$f(x) = \mu_y w \sigma \quad (4.19)$$

where  $\mu_y$  = the lateral friction coefficient

$\sigma$  = the normal pressure distribution under the track

The direction of lateral resistance is perpendicular to the track, and opposite to the slip direction of the track as shown in Fig. 4.5 in the next section. However, it is more convenient to represent the lateral resistance as single concentrate force in y-direction by integrate  $f(x)$  of both tracks over the length of the tracks as given below:

$$F_f = \text{sign}(\omega) \bullet \left[ \int_{-l/2}^d (f_R(x) + f_L(x)) dx - \int_d^{l/2} (f_R(x) + f_L(x)) dx \right] \quad (4.20)$$

*Moment of Turning Resistance,  $M_r$ :*

By referring to Fig. 4.5, the resultant moment of the lateral resistance on both tracks about the z-axis can be determined by

$$M_r = \text{sign}(\omega) \bullet \left[ \int_{-l/2}^d x(f_R(x) + f_L(x)) dx - \int_d^{l/2} x(f_R(x) + f_L(x)) dx \right] \quad (4.21)$$

The direction of the moment of turning resistance will be opposite to the direction of the angular velocity of the tracked vehicle.



the instantaneous center can be shifted forward or backward from the center of the tracks. The amount of shifting is denoted as  $d$  in Fig. 4.5, and can be determined from:

$$d = -\frac{v_y}{\omega}, \text{ when } \omega \neq 0 \quad (4.22)$$

$$\text{where } -\frac{l}{2} \leq d \leq \frac{l}{2}$$

The radius of turning ( $R_t$ ) of the tracked vehicle is the distance from the instantaneous center to the geometric center of the tracked vehicle, and can be calculated from the following expression.

$$R_t = \sqrt{d^2 + \left(\frac{v_x}{\omega}\right)^2}, \text{ when } \omega \neq 0 \quad (4.23)$$

From Fig. 3.1, 4.2, and 4.5, the equations of motion of the MBC maneuvered over flat ground in the global coordinate system can be written as:

$$mA_{G,X} = \sum F_x \cos(\theta) - \sum F_y \sin(\theta) \quad (4.24)$$

$$mA_{G,Y} = \sum F_x \sin(\theta) + \sum F_y \cos(\theta) \quad (4.25)$$

$$I_G \alpha_G = \sum M + mA_X e \sin(\beta) - mA_Y e \cos(\beta) \quad (4.26)$$

where

$$\sum F_x = F_R + F_L - (R_R + R_L) + F_{f,x} + F_{r,x}$$

$$\sum F_y = F_f + F_{f,y} + F_{r,y}$$

$$\sum M = \frac{B}{2}(F_R - F_L - R_R + R_L) + F_{f,y}e_D - F_{r,y}e_r + M_r$$

$$e = \sqrt{e_x^2 + e_y^2}$$

$$\beta = \theta + \text{ARCTAN2}(e_y, e_x)$$

$m$  = mass of the MBC

$I_G$  = mass moment of inertia of the MBC at the center of gravity with respect to the z-axis

$A_{G,X}$  and  $A_{G,Y}$  = Linear accelerations at the center of gravity

$\alpha_G =$  Angular acceleration at the center of gravity

Eqs. 4.24 to 4.26 yield the linear and angular accelerations of the MBC at the center of gravity. To relate these accelerations to determine the accelerations at the geometric center of the MBC, the following equations may be used.

$$A_x = A_{G,x} + \alpha_G (e_x \sin(\theta) + e_y \cos(\theta)) - \omega^2 (e_y \sin(\theta) - e_x \cos(\theta)) \quad (4.27)$$

$$A_y = A_{G,y} + \alpha_G (e_y \sin(\theta) - e_x \cos(\theta)) + \omega^2 (e_x \sin(\theta) + e_y \cos(\theta)) \quad (4.28)$$

$$\alpha = \alpha_G \quad (4.29)$$

Once the accelerations of the tracked vehicle are obtained, the update of the velocities and position of the tracked vehicle for the next time step in the simulation program can be determined by numerically integrating the accelerations and velocities over a period of time step( $\Delta t$ ), respectively.

### 4.3 The System of Equations of Motion of the CHS

In this research, the development of a system of equations of motion of a multi-unit tracked vehicle such as the CHS is based on the following assumptions:

- (1) The centers of gravity of MBCs are located at the geometric centers of MBCs.
- (2) The forces in the xy-plane acting at both connecting pins of an MBC do not affect the distributions of normal pressure beneath the tracks. Only the forces at the pins in z-direction due to the Pigs' weight will be taken into account.
- (3) The friction forces occurring between the Dollys and the MBCs are uniformly distributed over the contact area. The friction coefficient,  $\mu$ , is constant, and no stiction phenomenon is concerned. The friction forces presenting at the connecting pins are neglected.
- (4) The Dollys' travel limits are modeled by using variable friction coefficients instead of modeling them as real physical limits.

The first and second assumptions are very useful because they help in simplifying the system of equations of motion. The accelerations at the geometric center of the MBCs are the same as those at the center of gravity due to the first assumption; as a result, eqs. 4.27 and 4.28 need not to be employed. Since the normal pressure distributions beneath the tracks are independent to the connecting pin forces in the xy-plane according to the second assumption, the expressions of the tractive effort of the tracks can be greatly simplified. The second assumption is valid because the values of pin forces in the xy-plane are much less than the MBC's and Pigs' weight. The moment due to friction forces at the Dollies can be neglected because of the third assumption. The last assumption is made to reduce the complication of reforming new matrices containing the equations of motion of the system every time when the system losses some degrees of freedom because the Dollies hit the travel limits.

All assumptions above are made to simplify the system model, and, sometime, it seems to be oversimplified. Nevertheless, even we have not validated the CHS model, yet the simulations yield the satisfactory and reasonable results. The model validation in this case is difficult and costly, so we ignore the validation of the system model. Moreover, we decide to control the CHS by controlling each of the MBCs using separated controllers instead of trying to control the whole system using single controller. Therefore, even the accuracy of the system model is slightly reduced, we still can use the model to study the main dynamic characteristics of the system.

*Deriving the system of equations of motion of the CHS:*

From Fig. 3.5, each component in the partial chain of the CHS can be shown separately in a free-body diagram and an acceleration diagram as shown in Fig. 4.6 and 4.7 respectively. From the free-body diagrams, the equations of motion for each component may be written as follows:

$i^{\text{th}}$  MBC:

$$m_i A_{X,i} = F_{x,i} \cos(\theta_i) - F_{y,i} \sin(\theta_i) + F_{PMX,i} \quad (4.30)$$

$$m_i A_{Y,i} = F_{x,i} \sin(\theta_i) + F_{y,i} \cos(\theta_i) + F_{PMY,i} \quad (4.31)$$

$$I_i \alpha_i = M_i - e_{r,i} \cos(\theta_i) F_{PMY,i} + e_{r,i} \sin(\theta_i) F_{PMX,i} \quad (4.32)$$

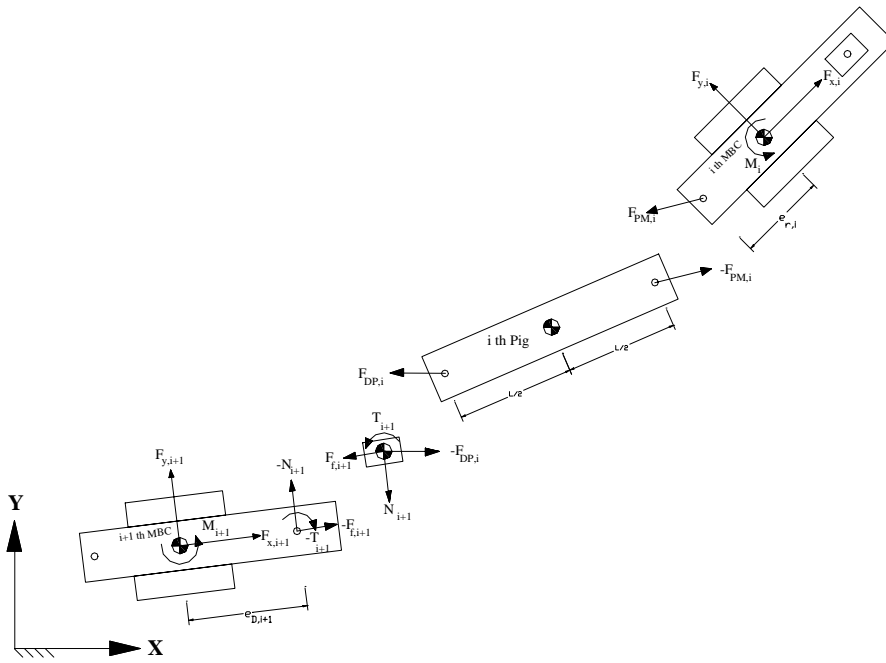


Figure 4.6. Free-Body Diagrams

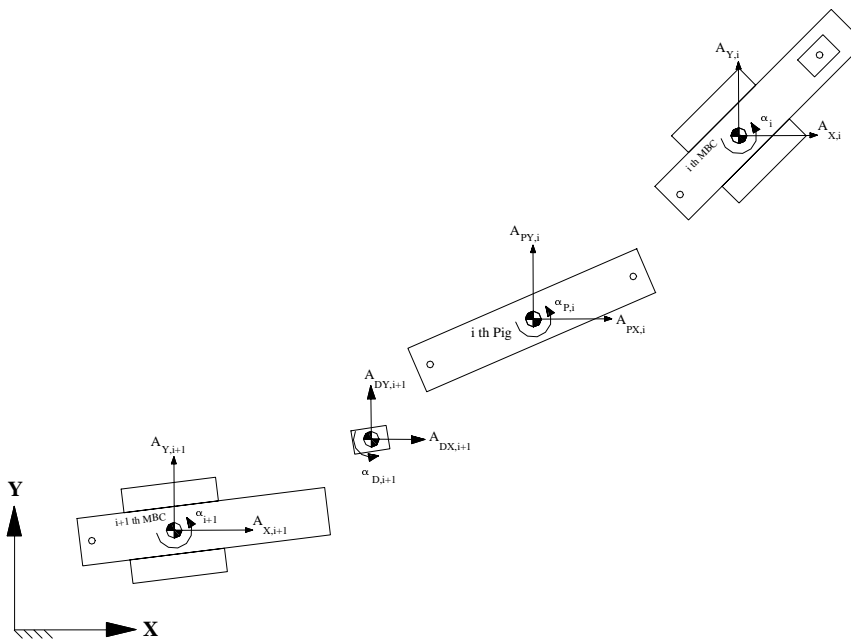


Figure 4.7. Acceleration Diagrams

where

$$F_{x,i} = F_{R,i} + F_{L,i} - (R_{R,i} + R_{L,i}) + F_{f,xi} + F_{r,xi}$$

$$F_{y,i} = F_{f,i} + F_{f,yi} + F_{r,yi}$$

$$M_i = \frac{B}{2}(F_{R,i} - F_{L,i} - R_{R,i} + R_{L,i}) + F_{f,yi}e_{D,i} - F_{r,yi}e_{r,i} + M_{r,i}$$

$i^{\text{th}}$  Pig:

$$m_{P,i}A_{PX,i} = -F_{PMX,i} + F_{DPX,i} \quad (4.33)$$

$$m_{P,i}A_{PY,i} = -F_{PMY,i} + F_{DPY,i} \quad (4.34)$$

$$I_{P,i}\alpha_{P,i} = -\frac{L}{2}\cos(\theta_{P,i})F_{PMY,i} + \frac{L}{2}\sin(\theta_{P,i})F_{PMX,i} - \frac{L}{2}\cos(\theta_{P,i})F_{DPY,i} + \frac{L}{2}\sin(\theta_{P,i})F_{DPX,i} \quad (4.35)$$

$i+1^{\text{th}}$  Dolly:

$$m_{D,i+1}A_{DX,i+1} = N_{i+1}\sin(\theta_{i+1}) - F_{DPX,i} - \text{sign}(v_{D,i+1})\mu \left[ |N_{i+1}| + (m_{D,i+1} + \frac{m_{P,i}}{2})g \right] \cos(\theta_{i+1}) \quad (4.36)$$

$$m_{D,i+1}A_{DY,i+1} = -N_{i+1}\cos(\theta_{i+1}) - F_{DPY,i} - \text{sign}(v_{D,i+1})\mu \left[ |N_{i+1}| + (m_{D,i+1} + \frac{m_{P,i}}{2})g \right] \sin(\theta_{i+1}) \quad (4.37)$$

$$I_{D,i+1}\alpha_{D,i+1} = T_{i+1} \quad (4.38)$$

$i+1^{\text{th}}$  MBC:

$$m_{i+1}A_{X,i+1} = F_{x,i+1}\cos(\theta_{i+1}) - F_{y,i+1}\sin(\theta_{i+1}) + \text{sign}(v_{D,i+1})\mu \left[ |N_{i+1}| + (m_{D,i+1} + \frac{m_{P,i}}{2})g \right] \cos(\theta_{i+1}) - N_{i+1}\sin(\theta_{i+1}) \quad (4.39)$$

$$m_{i+1}A_{Y,i+1} = F_{x,i+1}\sin(\theta_{i+1}) + F_{y,i+1}\cos(\theta_{i+1}) + \text{sign}(v_{D,i+1})\mu \left[ |N_{i+1}| + (m_{D,i+1} + \frac{m_{P,i}}{2})g \right] \sin(\theta_{i+1}) + N_{i+1}\cos(\theta_{i+1}) \quad (4.40)$$

$$I_{i+1}\alpha_{i+1} = M_{i+1} - T_{i+1} + e_{D,i+1}N_{i+1} \quad (4.41)$$

In the above equations, there are twelve unknowns needed to be solved:  $A_{X,i}$ ,  $A_{Y,i}$ ,  $\alpha_i$ ,  $A_{X,i+1}$ ,  $A_{Y,i+1}$ ,  $\alpha_{i+1}$ ,  $F_{PMX,i}$ ,  $F_{PMY,i}$ ,  $F_{DPX,i}$ ,  $F_{DPY,i}$ ,  $N_{i+1}$ , and  $T_{i+1}$ . We also have twelve equations of motion; therefore, these equations just need to be cast in the matrix form and solved by a digital computer. However, before these equations can be expressed in the matrix form, the linear and angular accelerations of the Pig and Dolly have to be written in terms of the accelerations of the MBCs ( $A_{X,i}$ ,  $A_{Y,i}$ ,  $\alpha_i$ ,  $A_{X,i+1}$ ,  $A_{Y,i+1}$ , and  $\alpha_{i+1}$ ) as follows.

First, from the previous chapter, the acceleration analysis of an MBC yields:

$$a_{D,i+1} = \frac{F'B' - E'C'}{D'B' - E'A'} \quad (4.42)$$

, which can be written in the following form:

$$a_{D,i+1} = a_{i+1}(A_{X,i} - A_{X,i+1}) + b_{i+1}(A_{Y,i} - A_{Y,i+1}) + c_{i+1}\alpha_i + d_{i+1}\alpha_{i+1} + e_{i+1} \quad (4.43)$$

where

$$a_{i+1} = \frac{\cos(\theta_{P,i})}{\cos(\theta_{P,i} - \theta_{i+1})}$$

$$b_{i+1} = \frac{\sin(\theta_{P,i})}{\cos(\theta_{P,i} - \theta_{i+1})}$$

$$c_{i+1} = -\frac{e_{r,i} \sin(\theta_{P,i} - \theta_i)}{\cos(\theta_{P,i} - \theta_{i+1})}$$

$$d_{i+1} = -\frac{e_{D,i+1} \sin(\theta_{P,i} - \theta_{i+1})}{\cos(\theta_{P,i} - \theta_{i+1})}$$

$$e_{i+1} = \frac{e_{D,i+1}\omega_{i+1}^2 \cos(\theta_{P,i} - \theta_{i+1}) + e_{r,i}\omega_i^2 \cos(\theta_{P,i} - \theta_i) - 2v_{D,i+1}\omega_{i+1} \sin(\theta_{P,i} - \theta_{i+1}) + \omega_{P,i}^2 L}{\cos(\theta_{P,i} - \theta_{i+1})}$$

Also, from the acceleration analysis of the MBC, we get

$$\alpha_{P,i} = \frac{D'C' - F'A'}{D'B' - E'A'} \quad (4.44)$$

, which can be expressed in the following form:

$$\alpha_{P,i} = a_i(A_{X,i} - A_{X,i+1}) + b_i(A_{Y,i} - A_{Y,i+1}) + c_i\alpha_i + d_i\alpha_{i+1} + e_i \quad (4.45)$$

where

$$\begin{aligned} a_i &= -\frac{\sin(\theta_{i+1})}{L \cos(\theta_{P,i} - \theta_{i+1})} \\ b_i &= -\frac{\cos(\theta_{i+1})}{L \cos(\theta_{P,i} - \theta_{i+1})} \\ c_i &= -\frac{e_{r,i} \cos(\theta_i - \theta_{i+1})}{L \cos(\theta_{P,i} - \theta_{i+1})} \\ d_i &= -\frac{e_{D,i+1}}{L \cos(\theta_{P,i} - \theta_{i+1})} \\ e_i &= \frac{e_{r,i} \omega_i^2 \sin(\theta_{i+1} - \theta_i) + L \omega_{P,i}^2 \sin(\theta_{i+1} - \theta_{P,i}) + 2v_{D,i+1} \omega_{i+1}}{L \cos(\theta_{P,i} - \theta_{i+1})} \end{aligned}$$

Now, the equations of the linear accelerations at the center of gravity of a Dolly, Eqs. 3.17 and 3.18, can be rewritten respectively as follows:

$$\begin{aligned} A_{DX,i+1} &= M_{DX,i+1} A_{X,i} + N_{DX,i+1} A_{Y,i} + O_{DX,i+1} \alpha_i + P_{DX,i+1} A_{X,i+1} + Q_{DX,i+1} A_{Y,i+1} + R_{DX,i+1} \alpha_{i+1} \\ &\quad + S_{DX,i+1} \end{aligned} \quad (4.46)$$

$$\begin{aligned} A_{DY,i+1} &= M_{DY,i+1} A_{X,i} + N_{DY,i+1} A_{Y,i} + O_{DY,i+1} \alpha_i + P_{DY,i+1} A_{X,i+1} + Q_{DY,i+1} A_{Y,i+1} + R_{DY,i+1} \alpha_{i+1} \\ &\quad + S_{DY,i+1} \end{aligned} \quad (4.47)$$

where

$$\begin{aligned} M_{DX,i+1} &= a_{i+1} \cos(\theta_{i+1}) \\ N_{DX,i+1} &= b_{i+1} \cos(\theta_{i+1}) \\ O_{DX,i+1} &= c_{i+1} \cos(\theta_{i+1}) \\ P_{DX,i+1} &= 1 - a_{i+1} \cos(\theta_{i+1}) \\ Q_{DX,i+1} &= -N_{DX,i+1} \end{aligned}$$

$$\begin{aligned}
R_{DX,i+1} &= d_{i+1} \cos(\theta_{i+1}) - e_{D,i+1} \sin(\theta_{i+1}) \\
S_{DX,i+1} &= e_{i+1} \cos(\theta_{i+1}) - e_{D,i+1} \omega_{i+1}^2 \cos(\theta_{i+1}) - 2v_{D,i+1} \omega_{i+1} \sin(\theta_{i+1}) \\
, \text{ and} \\
M_{DY,i+1} &= a_{i+1} \sin(\theta_{i+1}) \\
N_{DY,i+1} &= b_{i+1} \sin(\theta_{i+1}) \\
O_{DY,i+1} &= c_{i+1} \sin(\theta_{i+1}) \\
P_{DY,i+1} &= -M_{DY,i+1} \\
Q_{DY,i+1} &= 1 - b_{i+1} \sin(\theta_{i+1}) \\
R_{DY,i+1} &= d_{i+1} \sin(\theta_{i+1}) + e_{D,i+1} \cos(\theta_{i+1}) \\
S_{DY,i+1} &= e_{i+1} \sin(\theta_{i+1}) - e_{D,i+1} \omega_{i+1}^2 \sin(\theta_{i+1}) + 2v_{D,i+1} \omega_{i+1} \cos(\theta_{i+1})
\end{aligned}$$

Repeating the whole process, the equations of the linear accelerations at the center of gravity of a Pig, Eqs. 3.24 and 3.25, can be written as follows:

$$A_{PX,i} = M_{PX,i} A_{X,i} + N_{PX,i} A_{Y,i} + O_{PX,i} \alpha_i + P_{PX,i} A_{X,i+1} + Q_{PX,i} A_{Y,i+1} + R_{PX,i} \alpha_{i+1} + S_{PX,i} \quad (4.48)$$

$$A_{PY,i} = M_{PY,i} A_{X,i} + N_{PY,i} A_{Y,i} + O_{PY,i} \alpha_i + P_{PY,i} A_{X,i+1} + Q_{PY,i} A_{Y,i+1} + R_{PY,i} \alpha_{i+1} + S_{PY,i} \quad (4.49)$$

where

$$M_{PX,i} = 1 + \frac{L}{2} a_i \sin(\theta_{P,i})$$

$$N_{PX,i} = -\frac{L}{2} b_i \sin(\theta_{P,i})$$

$$O_{PX,i} = e_{r,i} \sin(\theta_i) + \frac{L}{2} c_i \sin(\theta_{P,i})$$

$$P_{PX,i} = -\frac{L}{2} a_i \sin(\theta_{P,i})$$

$$Q_{PX,i} = -N_{PX,i}$$

$$R_{PX,i} = \frac{L}{2} d_i \sin(\theta_{P,i})$$

$$S_{PX,i} = \frac{L}{2} e_i \sin(\theta_{P,i}) + e_{r,i} \omega_i^2 \cos(\theta_i) + \frac{L}{2} \omega_{P,i}^2 \cos(\theta_{P,i})$$

, and

$$M_{PY,i} = -\frac{L}{2} a_i \cos(\theta_{P,i})$$

$$N_{PY,i} = 1 + \frac{L}{2} b_i \sin(\theta_{P,i})$$

$$O_{PY,i} = -(e_{r,i} \cos(\theta_i) + \frac{L}{2} c_i \cos(\theta_{P,i}))$$

$$P_{PY,i} = -M_{PY,i}$$

$$Q_{PY,i} = -\frac{L}{2} b_i \cos(\theta_{P,i})$$

$$R_{PY,i} = -\frac{L}{2} d_i \cos(\theta_{P,i})$$

$$S_{PY,i} = -\frac{L}{2} e_i \cos(\theta_{P,i}) + e_{r,i} \omega_i^2 \sin(\theta_i) + \frac{L}{2} \omega_{P,i}^2 \sin(\theta_{P,i})$$

*Forming the system matrix:*

Substituting Eqs. 4.46 to 4.49 into Eqs. 4.33, 4.34, 4.36, and 4.37, one can express Eqs. 4.30 through 4.41 in the matrix form shown below.

$$[A]\{x\} = \{y\} \quad (4.50)$$

$$[A] =$$

$$\begin{bmatrix} m^i & 0 & 0 & -1 & 0 & 0 & 0 & 0 & 0 & 0 & 0 & 0 & 0 \\ 0 & m^i & 0 & 0 & -1 & 0 & 0 & 0 & 0 & 0 & 0 & 0 & 0 \\ 0 & 0 & I^i & -e^{r,i} s \theta^i & e^{r,i} c \theta^i & 0 & 0 & 0 & 0 & 0 & 0 & 0 & 0 \\ m^{P,i} M^{PX,i} & m^{P,i} N^{PX,i} & m^{P,i} O^{PX,i} & 1 & 0 & -1 & 0 & 0 & 0 & m^{P,i} P^{PX,i} & m^{P,i} Q^{PX,i} & m^{P,i} R^{PX,i} \\ m^{P,i} M^{PY,i} & m^{P,i} N^{PY,i} & m^{P,i} O^{PY,i} & 0 & 1 & 0 & -1 & 0 & 0 & m^{P,i} P^{PY,i} & m^{P,i} Q^{PY,i} & m^{P,i} R^{PY,i} \\ I^{P,i} a^i & -I^{P,i} b^i & I^{P,i} c^i & -\frac{\tau}{2} s \theta^{P,i} & \frac{\tau}{2} c \theta^{P,i} & -\frac{\tau}{2} s \theta^{P,i} & \frac{\tau}{2} c \theta^{P,i} & 0 & 0 & -I^{P,i} a^i & I^{P,i} b^i & I^{P,i} d^i \\ m^{D,i+1} M^{DX,i+1} & m^{D,i+1} N^{DX,i+1} & m^{D,i+1} O^{DX,i+1} & 0 & 0 & 1 & 0 & 0 & A & m^{D,i+1} P^{DX,i+1} & m^{D,i+1} Q^{DX,i+1} & m^{D,i+1} R^{DX,i+1} \\ m^{D,i+1} M^{DY,i+1} & m^{D,i+1} N^{DY,i+1} & m^{D,i+1} O^{DY,i+1} & 0 & 0 & 0 & 1 & 0 & B & m^{D,i+1} P^{DY,i+1} & m^{D,i+1} Q^{DY,i+1} & m^{D,i+1} R^{DY,i+1} \\ 0 & 0 & 0 & 0 & 0 & 0 & 0 & 0 & 0 & -1 & 0 & 0 & I^{D,i+1} \\ 0 & 0 & 0 & 0 & 0 & 0 & 0 & 0 & 0 & C & 0 & 0 & m^{i+1} \\ 0 & 0 & 0 & 0 & 0 & 0 & 0 & 0 & 0 & D & 0 & 0 & m^{i+1} \\ 0 & 0 & 0 & 0 & 0 & 0 & 0 & 0 & -e^{D,i+1} & 1 & 0 & 0 & I^{i+1} \end{bmatrix}$$

where

$$A = -\sin(\theta_{i+1}) + \text{sign}(v_{D,i+1})\text{sign}(N_{i+1})\mu \cos(\theta_{i+1})$$

$$B = \cos(\theta_{i+1}) + \text{sign}(v_{D,i+1})\text{sign}(N_{i+1})\mu \sin(\theta_{i+1})$$

$$C = \sin(\theta_{i+1}) - \text{sign}(v_{D,i+1})\text{sign}(N_{i+1})\mu \cos(\theta_{i+1})$$

$$D = -B$$

The unknowns are arranged in the unknown vector,  $\{x\}$ , as follows:

$$\begin{Bmatrix} A_{X,i} \\ A_{Y,i} \\ \alpha_i \\ F_{PMX,i} \\ F_{PMY,i} \\ F_{DPX,i} \\ F_{DPY,i} \\ N_{i+1} \\ T_{i+1} \\ A_{X,i+1} \\ A_{Y,i+1} \\ \alpha_{i+1} \end{Bmatrix}$$

The constant vector,  $\{y\}$ , is shown below.

$$\begin{Bmatrix} F_{x,i} \cos(\theta_i) - F_{y,i} \sin(\theta_i) \\ F_{x,i} \sin(\theta_i) + F_{y,i} \cos(\theta_i) \\ M_i \\ -S_{PX,i} \\ -S_{PY,i} \\ -I_{P,i} e_i \\ -S_{DX,i+1} - \text{sign}(v_{D,i+1})\mu \left[ (m_{D,i+1} + \frac{m_{P,i}}{2})g \right] \cos(\theta_{i+1}) \\ -S_{DY,i+1} - \text{sign}(v_{D,i+1})\mu \left[ (m_{D,i+1} + \frac{m_{P,i}}{2})g \right] \sin(\theta_{i+1}) \\ 0 \\ F_{x,i+1} \cos(\theta_{i+1}) - F_{y,i+1} \sin(\theta_{i+1}) + \text{sign}(v_{D,i+1})\mu \left[ (m_{D,i+1} + \frac{m_{P,i}}{2})g \right] \cos(\theta_{i+1}) \\ F_{x,i+1} \sin(\theta_{i+1}) + F_{y,i+1} \cos(\theta_{i+1}) + \text{sign}(v_{D,i+1})\mu \left[ (m_{D,i+1} + \frac{m_{P,i}}{2})g \right] \cos(\theta_{i+1}) \\ M_{i+1} \end{Bmatrix}$$

The dimension of the matrix will be expanded when more MBC-Pig pairs are added to the system or vice versa, which can be easily done in a digital computer. There is one interesting point about solving this system of linear equations because there are the absolute values of the normal forces,  $N_{i+1}$ , presenting on the left side of Eqs. 4.36, 4.37, 4.39, and 4.40. Since the directions of the friction forces depend solely on the moving directions of the Dollys, the values of normal forces can be either positive or negative and still yield the same values of friction forces. To prevent this ambiguity, the expected signs of direction of those normal forces must be guessed before the system matrix can be generated. After the system matrix has been solved, the sign agreement checking has to be done to determine whether the further guessing is needed. This makes the simulation time increase drastically due to the increasing of the number of matrices, which have to be formed every trials in one time step, when the number of the MBC-Pig pairs are increased. The number of guessing times can be calculated from the following expression.

$$n = 2^N \quad (4.51)$$

where  $n$  = number of guessing

$N$  = number of the normal forces

Moreover, the guessing process brings about the problem that the total elapsed time of the simulation cannot be exactly specified because of the uncertainty of the amount of guessing taking place in each time step. Nevertheless, the simulation is not used for performing a real-time simulation, so it is acceptable in this case to have the variation of the total simulation time.

#### **4.4 The Simplified Model of the Dolly Travel Limit**

Whenever the MBC's dolly reaches the ends of travel range, the system or the CHS loses one degree of freedom. Therefore, if one would directly model the actual physical situation occurred, some elements of the system matrix have to be rederived. Since the system loses some degrees of freedom at the Dollys, the dimension of the system matrix is reduced. The constrained Dollys are modelled as they are just the

ordinary connecting pins. Moreover, a subroutine used to monitor whether or not the Dollies reach their travel limits is required.

To avoid these complications, a simplified model of the Dolly travel limit is proposed. The idea is to use the friction coefficient ( $\mu$ ) that varies over the travel range of the Dolly. The value of the friction coefficient will be increased exponentially when the Dolly moves close to the travel limits, denoted as “End Zone” in Fig. 4.8.

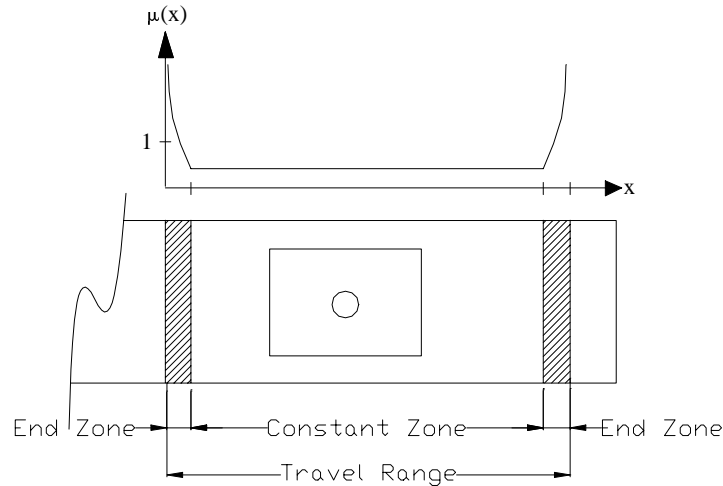


Figure 4.8. The Variation of Friction Coefficient

This simplified model can be directly applied to the existing system model; therefore, no major effort is needed in modifying the simulation code. After many experiments had been done to examine the simulation program, the simplified model seems to work very well by yielding reasonable simulation results. However, the drawback of this approach is that those constant( or variable) in the exponential function used to evaluate the friction coefficient can be obtained only by trial-and-error method. The suitable values of the constants must yield the maximum friction coefficient, yet prevent the system matrix from being badly scaled.